HEFAT 2014
10th International Conference on Heat Transfer, Fluid Mechanics and Thermodynamics
14-16 July 2014
Orlando, Florida

ANALYSIS OF THERMAL MIXING VIA BEJAN'S HEATLINE DURING NATURAL CONVECTION WITHIN SQUARE CAVITIES WITH DISCRETE HEAT SOURCES

Das D. and Basak T.*
* Author for correspondence

Department of Chemical Engineering,
Indian Institute of Technology Madras,
Chennai - 600036,
India
Email: tanmay@iitm.ac.in

1 ABSTRACT

Natural convection is the governing phenomena in many engineering applications. The conventional method of differential heating of an enclosure may result in inadequate thermal mixing and poor temperature distribution leading to high amount of energy loss. In the present study, an alternative, energy-efficient method of distributed heating of the cavity is studied and compared with the differential heating case in enhancing the thermal mixing and improving the temperature distribution in the cavity. Six different cases, depending upon the location of the heat sources on the side walls of the cavity, are studied. Fluids with $Pr = 7$ have been investigated at high Rayleigh number ($Ra = 10^3 - 10^5$). Galerkin finite element method has been implemented for solving the governing equations and Poisson-type of equations for streamfunction and heatfunction. Heatlines are found to be adequate tools for visualizing and understanding the heat energy distribution occurring inside a cavity. It is found that thermal management policy of distributed heating significantly influences the thermal mixing and temperature uniformity in the enclosures.

2 INTRODUCTION

Classical differential heating involves one isothermally hot side wall while other side wall is maintained isothermally cold in presence of adiabatic horizontal walls [1]. Natural convection in various enclosures with differential heating has been studied by various authors [2, 3] as these types of configurations are found to be useful in applications such as geothermal phenomena and the safe disposal of nuclear waste. At steady state, thermal gradient in this type of configuration may lead to the formation of hot and cold regimes. These might enhance the chances of formation of hot spots and cold spots which may be undesirable for the processes where temperature uniformity is a critical parameter for efficient processing.

Earlier workers studied the approach of discrete/distributed heating, which is considered as a potential methodology over differential heating for enhanced thermal processing of materials [4]. The buoyancy flow induced by discrete heat sources from multiple locations results in improved mixing throughout the enclosure minimizes the formation of hotspots and coldspots [5]. Thus, the process of discrete/distributed heating has advantages such as improved mixing, better temperature uniformity, better control over flow field and most importantly, high energy efficiency. Several industrial applications are reported in the literature [6, 7], where the concept of distributed heating has been employed for enhanced thermal mixing of fluid.

NOMENCLATURE

g	[m/s^2]	acceleration due to gravity
k	[W/mK]	thermal conductivity
l	[-]	dimensionless length of hot/cold part
L	[m]	side of the square cavity
N	[-]	total number of nodes
$\overline{Nu}$	[-]	average Nusselt number
p	[Pa]	pressure
P	[-]	dimensionless pressure
Pr	[-]	Prandtl number
Ra	[-]	Rayleigh number
$RMSD$	[-]	root-mean square deviation
T	[K]	temperature
T_h	[K]	temperature of hot right wall
T_c	[K]	temperature of cold left wall
u	[m/s]	x component of velocity
U	[-]	x component of dimensionless velocity
v	[m/s]	y component of velocity
V	[-]	y component of dimensionless velocity
x	[m]	distance along x axis
X	[-]	dimensionless distance along x axis
y	[m]	distance along y axis
Y	[-]	dimensionless distance along y axis

Greek symbols

α	[m^2/s]	thermal diffusivity
β	[1/K]	volume expansion coefficient

γ	[-]	penalty parameter
θ, Θ	[-]	dimensionless temperature
ν	[m^2/s]	kinematic viscosity
ρ	[kg/m^3]	density
Φ	[-]	basis functions
Π	[-]	dimensionless heatfunction
ψ	[-]	dimensionless streamfunction

Subscripts

k	node number
l	left wall
r	right wall
$1, 3$	cold section
$2, 4$	hot section
cup	cup-mixing
avg	spatial average

In this work, visualization of heat flow via heatlines are elucidated for comprehensive understanding of thermal mixing due to discrete heat sources, which would immensely help in designing systems with high energy efficiency.

Most of the studies in enclosures with discrete heat sources in literature are analyzed and illustrated using streamlines and isotherms [8]. Streamlines are found to be adequate in describing the fluid flow, but isotherms are inadequate to study energy flow, as the isotherm contours indicate only temperature variations which are sufficient enough to study conduction heat transfer.

In order to analyze convective heat transfer and heat flow distributions, there is a demand for proper tool which can be used for the visualization of energy flow inside an enclosure. One such mathematical tool termed as, 'heatlines' was developed by Kimura and Bejan [9]. The 'heatlines', analogous to streamlines, are trajectories of flow of heat and thus, they are useful to visualize the total energy flow in a two-dimensional domain.

The main aim of the present work is to investigate the scope of application of distributed heating over conventional differential heating for enhancing the thermal mixing during material processing through the understanding of fluid flow, heat flow and their influence on temperature distribution during natural convection in enclosures filled with clear fluid. Six different cases with various locations of discrete heat sources on the walls of the cavity were considered. Representative cases are illustrated in Figure 1. To asses the performance in terms of achieving enhanced thermal mixing and maximum heat transfer rate quantitatively, 'cup mixing temperature' and 'average temperature' have been calculated for all the cases. The efficacy of distributed heating over conventional differential heating for optimal thermal mixing is established by correlating heatlines and 'cup-mixing temperature'. Overall uniformity in temperature and degree of mixing inside the enclosure is further quantified using 'root mean square deviation ($RMSD$)'.

3 MATHEMATICAL FORMULATION AND SIMULATION

The physical domains of the square enclosure with the distributed heating sources are given in Figure $1a-c$. Isothermal heat sources are distributed along the side walls of the

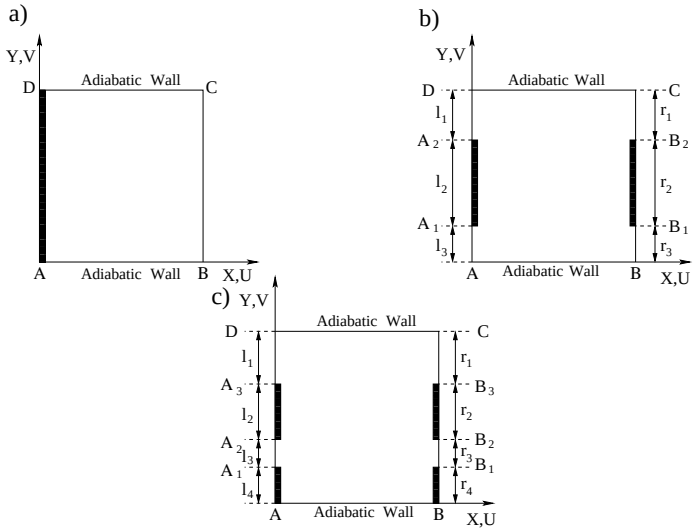

Figure 1: Schematic diagram of the cavity for a) differential heating case b) case $1-4$ c) case $5-6$. Top and bottom walls are adiabatic. Thick lines represent the uniformly heated section while remaining sections are maintained cold

cavity, which are represented by thick solid lines. Remaining portions of the cavity are maintained isothermally cold except the top and the bottom insulated wall. It may be noted that, for all the six cases, the total dimensionless length of the heat source is 1. The first four cases (case $1-4$) involve single slot distributed heating system with various orientations of heaters, each of length 0.5, on the side walls (see Table $1a$). The last two cases (case $5-6$) involve the different positioning of multiple slot heating system on the side walls such that the total heater length on each side wall is equal to 0.5. Representative schematic diagrams are shown for the differential heating case (Fig. $1a$), case 1-4 (Fig. $1b$) and case 5-6 (Fig. $1c$).

Table 1a: Length of the hot and cold zone along the side walls for single slot (Case $1-4$) distributed heating system.

Enclosure	AA_1	A_2D	BB_1	B_2C
Case 1	0.5	–	0.5	–
Case 2	0.15	0.35	0.15	0.35
Case 3	0.25	0.25	0.25	0.25
Case 4	0.15	0.35	0.35	0.15

Table 1b: Length of the hot and cold zone along the side walls for multiple slot (Case $5-6$) distributed heating system.

Enclosure	AA_1	A_1A_2	A_2A_3	BB_1	B_1B_2	B_2B_3
Case 5	0.35	0.5	–	0.35	0.5	–
Case 6	0.15	0.15	0.35	0.15	0.15	0.35

Based on assumptions as stated in an earlier work [12], governing equations for steady two-dimensional natural convection flow in the square cavity using conservation of mass, momentum and energy can be written with following dimensionless variables or numbers:

$$X = \frac{x}{L}, \quad Y = \frac{y}{L}, \quad U = \frac{uL}{\alpha}, \quad V = \frac{vL}{\alpha}, \quad P = \frac{pL^2}{\rho\alpha^2},$$

$$\theta = \frac{T - T_c}{T_h - T_c}, \quad Pr = \frac{\nu}{\alpha}, \quad Ra = \frac{g\beta L^3 (T_h - T_c) Pr}{\nu^2} \quad (1)$$

$$\frac{\partial U}{\partial X} + \frac{\partial V}{\partial Y} = 0, \quad (2)$$

$$U\frac{\partial U}{\partial X} + V\frac{\partial U}{\partial Y} = -\frac{\partial P}{\partial X} + Pr\left(\frac{\partial^2 U}{\partial X^2} + \frac{\partial^2 U}{\partial Y^2}\right), \quad (3)$$

$$U\frac{\partial V}{\partial X} + V\frac{\partial V}{\partial Y} = -\frac{\partial P}{\partial Y} + Pr\left(\frac{\partial^2 V}{\partial X^2} + \frac{\partial^2 V}{\partial Y^2}\right) + RaPr\theta, \quad (4)$$

$$U\frac{\partial \theta}{\partial X} + V\frac{\partial \theta}{\partial Y} = \frac{\partial^2 \theta}{\partial X^2} + \frac{\partial^2 \theta}{\partial Y^2} \quad (5)$$

The velocity boundary conditions are given as follows:

$$\begin{aligned} U(X,0) &= U(X,1) = U(0,Y) = U(1,Y) = 0 \\ V(X,0) &= V(X,1) = V(0,Y) = V(1,Y) = 0 \end{aligned} \quad (6)$$

and the boundary conditions for temperature for all the cases are as follows:

$$\begin{aligned} \theta &= 1 \text{ (for the hot zone)} \\ &= 0 \text{ (for the cold zone)} \\ \frac{\partial \theta}{\partial Y} &= 0 \text{ (for the top and bottom adiabatic walls)} \end{aligned} \quad (7)$$

Note that, in Eqs. 1-7, X and Y are dimensionless coordinates varying along the horizontal and vertical directions, respectively; U and V are dimensionless velocity components in the X and Y directions, respectively: θ is the dimensionless temperature; P is the dimensionless pressure; Ra and Pr are the Rayleigh and Prandtl numbers, respectively; T_h and T_c are the temperature at the hot and cold walls respectively; L is the side of the cavity.

3.1 Solution procedure

The momentum and energy balance equations (Eqs. 3 - 5) are solved using the Galerkin's finite element method. The continuity equation, Eq. 2 will be used as a constraint due to mass conservation and this constraint may be used to obtain the pressure distribution. In order to solve Eqs. 3,4, the penalty finite-element method is used [10], where the pressure (P) is eliminated by a penalty parameter (γ) and the incompressibility criteria is given by Eq. 2, which results in

$$P = -\gamma\left(\frac{\partial U}{\partial X} + \frac{\partial V}{\partial Y}\right), \quad (8)$$

The continuity equation, Eq. 2 is satisfied for higher values of γ. Typical values of γ that yield consistent solutions are 10^7. Using Eq. 8, the momentum balance equations (Eqs. 3 and 4) reduce to

$$U\frac{\partial U}{\partial X} + V\frac{\partial U}{\partial Y} = \gamma\frac{\partial}{\partial X}\left(\frac{\partial U}{\partial X} + \frac{\partial V}{\partial Y}\right) + Pr\left(\frac{\partial^2 U}{\partial X^2} + \frac{\partial^2 U}{\partial Y^2}\right), \quad (9)$$

$$U\frac{\partial V}{\partial X} + V\frac{\partial V}{\partial Y} = \gamma\frac{\partial}{\partial X}\left(\frac{\partial U}{\partial X} + \frac{\partial V}{\partial Y}\right) + Pr\left(\frac{\partial^2 U}{\partial X^2} + \frac{\partial^2 U}{\partial Y^2}\right) + RaPr\theta \quad (10)$$

3.2 Streamfunction and Heatfunction

3.2.1 Streamfunction

The streamfunction (ψ) can be used to plot streamlines, which represent the trajectories of particles in a steady flow and is obtained from velocity components U and V. The relationships between streamfunction and velocity components for two dimensional flows are

$$U = \frac{\partial \psi}{\partial Y} \text{ and } V = -\frac{\partial \psi}{\partial X}, \quad (11)$$

The combination of above relationships yields following single equation

$$\frac{\partial^2 \psi}{\partial X^2} + \frac{\partial^2 \psi}{\partial Y^2} = \frac{\partial U}{\partial Y} - \frac{\partial V}{\partial X}. \quad (12)$$

The positive sign of ψ denotes anti-clockwise circulation and negative sign represents the clockwise circulation. It may be noted that, no-slip condition ($\psi = 0$) is valid at all boundaries and there is no cross flow. The detailed solution procedure to solve Eq. 12 is given in an earlier work [11].

3.2.2 Heatfunction

The heatfunction (Π) can be used to plot heatlines, which represent the trajectories of heat flow and is obtained from conductive heat fluxes ($-\frac{\partial \theta}{\partial X}$, $-\frac{\partial \theta}{\partial Y}$) as well as convective heat fluxes ($U\theta$, $V\theta$). The heatfunction satisfies the steady energy balance equation Eq.(5) such that,

$$\frac{\partial \Pi}{\partial Y} = U\theta - \frac{\partial \theta}{\partial X} \text{ and } -\frac{\partial \Pi}{\partial X} = V\theta - \frac{\partial \theta}{\partial Y}. \quad (13)$$

The combination of above relationships yields a following single equation

$$\frac{\partial^2 \Pi}{\partial X^2} + \frac{\partial^2 \Pi}{\partial Y^2} = \frac{\partial}{\partial Y}(U\theta) - \frac{\partial}{\partial X}(V\theta) \quad (14)$$

It may be noted that, the solution of heatfunction is strongly dependent on non-homogeneous Dirichlet boundary condition. Also, the sign of heatfunction is governed by the sign of 'non-homogeneous' Dirichlet condition specified at the edges of the discrete heat sources. The sign convention for the heatlines are in agreement with that of streamlines. Further, it may be noted that the streamfunction and heatfunction have identical signs for convective transport.

Eq. 14 is further supplemented with various Dirichlet and Neumann boundary conditions in order to obtain an unique solution of Eq. 14. Neumann boundary conditions of Π, derived from Eq. 13 is specified as,

$$\mathbf{n} \cdot \nabla \Pi = 0 \quad (15)$$

The Dirichlet boundary condition for top insulated wall is obtained from Eq. 15 which is simplified into $\frac{\partial \Pi}{\partial X} = 0$ for an adiabatic wall. A reference value of Π is assumed to be 0 at $X = 0$, $Y = 1$ and hence $\Pi = 0$ is valid for $Y = 1$, for all X. It may be noted that, current work is based on situations of differential and distributed heating which correspond to various non-homogeneous Dirichlet conditions for

Π at the hot-cold junctions. The unique solution of Eq.14 is strongly dependent on the non-homogeneous Dirichlet conditions and the boundary conditions at these junctions are obtained by integrating Eq.13 along boundaries from the reference point until the end point of each junction. Representative calculations for multiple distributed heating (cases $5-6$) are given as follows:

Case 5 or 6:

(i) At D,

$$\Pi(D) = 0 \tag{16}$$

(ii) At A_3,

$$\begin{aligned} \Pi(A_3) &= \Pi(D) + \int_D^{A_3} \frac{\partial \Pi}{\partial Y} dY \\ &= l_1 \overline{Nu_{l1}} \end{aligned} \tag{17}$$

(iii) At A_2,

$$\begin{aligned} \Pi(A_2) &= \Pi(A_3) + \int_{A_3}^{A_2} \frac{\partial \Pi}{\partial Y} dY \\ &= \Pi(A_3) - l_2 \overline{Nu_{l2}} \end{aligned} \tag{18}$$

(iv) At A_1,

$$\begin{aligned} \Pi(A_1) &= \Pi(A_2) + \int_{A_2}^{A_1} \frac{\partial \Pi}{\partial Y} dY \\ &= \Pi(A_2) + l_3 \overline{Nu_{l3}} \end{aligned} \tag{19}$$

(v) At A,

$$\begin{aligned} \Pi(A) &= \Pi(A_1) + \int_{A_1}^{A} \frac{\partial \Pi}{\partial Y} dY \\ &= \Pi(A_1) - l_4 \overline{Nu_{l4}} \end{aligned} \tag{20}$$

Similarly, the value of $\Pi(B_3)$, $\Pi(B_2)$, $\Pi(B_1)$ and $\Pi(B)$ on the right wall are obtained. In an identical way, heat function boundary conditions for all other cases involving multiple slot distributed heating system have also been derived.

3.3 Cup mixing temperature and degree of temperature uniformity

To compare the thermal mixing in various cases, the bulk average temperature across the cavity also known as the 'cup-mixing temperature' is defined. Cup-mixing temperature is the velocity-weighted average temperature, which is most suitable when convective flow exists. The cup-mixing temperature (Θ_{cup}) and spatial average or area average temperature (Θ_{avg}) are given as:

$$\Theta_{cup} = \frac{\int\int \hat{V}(X,Y)\theta(X,Y)\, dXdY}{\int \hat{V}(X,Y)\, dXdY} \tag{21}$$

where,

$$\hat{V}(X,Y) = \sqrt{U^2 + V^2} \tag{22}$$

and

$$\Theta_{avg} = \frac{\int\int \theta(X,Y)\, dXdY}{\int dXdY} \tag{23}$$

Another quantity, namely 'Root Mean Square Deviation (RMSD)' is defined to quantify the degree of temperature uniformity in each case. Various forms of RMSD's are defined based on cup-mixing temperature (Θ_{cup}) and spatial average temperature (Θ_{avg}), as follows:

$$RMSD_{\Theta_i} = \sqrt{\frac{\sum_{k=1}^{N}(\theta_k - \Theta_i)^2}{N}} \tag{24}$$

where i = cup and average temperature, respectively. It may be noted that, $RMSD_{\Theta_{avg}}$ or $RMSD_{\Theta_{cup}}$ value cannot exceed 1 as the dimensionless temperature varies only between 0 and 1. Further, the lower values of RMSD indicate higher temperature uniformity in the cavity and vice-versa.

4 NUMERICAL TESTS

The computational domain consists of 28×28 bi-quadratic elements which correspond to 57×57 grid points. An adaptive grid with local refinement along X and Y near the discrete/distributed heat sources has been used. It may be noted that, for discrete heating cases, the hot wall is shared with the adjacent cold wall which may lead to jump discontinuities at the edges of the hot wall. To avoid this mathematical singularities at the hot edges, the average temperature of the two walls are specified at the hot-cold junction and the adjacent nodes are maintained at the respective wall temperatures. The unique solution for such type of situations involves implementation of exact boundary conditions at those singular points. Also, the current solution scheme produces grid invariant results as discussed in an earlier article [12]. Current Galerkin finite element approach offers special advantage on evaluation of local Nusselt number at the various cold or hot portions of the wall as element basis functions are used to evaluate the heat flux.

In order to validate the numerical procedure adopted for the solution of governing equations, the algorithm is tested for a square enclosure filled with water ($Pr = 0.71$) in presence of hot left wall and cold right wall with insulated top and bottom walls (differential heating) at $Ra = 10^5$, similar to the problem studied by Deng and Tang[1]. The results based on current simulation strategy (see Figure 2) are in excellent agreement with the earlier work [1]. Furthermore, in order to justify the physical explanation for heatlines, simulations are carried out for a wide range of Rayleigh numbers ($Ra = 10^3$ - 10^5) at $Pr = 7$ for various cases discussed in the following sections.

At $Ra = 10^3$, the fluid flow is found to be weak and the heat transfer occurs mainly due to conduction. It

Table 2: Comparisons of the present results with benchmark solution for natural convection in square cavity in presence of air ($Pr = 0.71$)

Ra	Present Work	Deng and Tang [1]
10^3	1.116	1.118
10^4	2.245	2.254
10^5	4.524	4.557

may be noted that, although circulation cells with streamfunction values occur for all the cases, there is no significant thermal mixing during conduction dominant regime. In the conduction dominant regime, heatlines essentially represented by 'heat-flux' lines, are perpendicular to the isothermal surfaces and parallel to the adiabatic surfaces. The heatlines originating from hot surface and ending on cold surface are observed to be orthogonal to isothermal surfaces. As they approach the top adiabatic wall, they slowly bend and become parallel to that surface. Heatlines are dense along the edges of the hot and cold wall denoting maximum heat transfer near the junctions. Also, heatlines and isotherms are smooth curves, without any distortion, which denote conduction dominant heat transport at low Ra ($Ra = 10^3$). Detailed analysis on streamlines, heatlines, isotherms and thermal mixing are shown for $Ra = 10^5$ for all the cases of distributed heating assemblies in section 5.

5 RESULTS AND DISCUSSIONS

5.1 Case 1

The distributions of streamlines, heatlines and isotherms at $Pr = 7$ and $Ra = 10^5$ are illustrated in Fig. 2. Isothermal heat sources are located at $0 \leq Y \leq 0.5$ along both the vertical walls. At high Ra ($Ra = 10^5$), the buoyancy forces start dominating over the viscous forces and circulations in the cavity are enhanced as seen from higher magnitudes of streamfunctions ($|\psi|_{max} = 6.7$). Due to hot bottom portion, fluid moves in upward direction. However, fluid does not reach the top portion, rather, fluid forms small circulation cell along the bottom portion. In a similar manner, anticlockwise circulation cell occurs at the bottom portion of the right half of the cavity. On the other hand, at the top portion, fluid near the hot layer zone around $Y = 0.5$, rises along the centerline and falls down along the cold walls at $1 \leq Y \leq 0.5$, thus forming cells in the top half of the cavity. Note that, streamline cells with identical magnitude, are observed at the left and right halves of the cavity. As seen from the signs of sreamfunction, counter rotating circulation cells occur at each of the left and right portion of the cavity (see Fig. 2).

Heatlines show several interesting trends at high Ra. Due to high convective effect, heatlines are similar to streamlines in 90% of the cavity except near the walls. End to end heatlines emanate from the heaters and travel a longer path to deliver heat from the hot bottom portion to the cold top portion of the side walls (see Fig. 2). This results in formation of sparse heatlines at the upper middle portion of side walls depicting very less heat transfer. It is interesting to observe that the heatlines near the top portion of the side walls vary within $0.1 - 1.2$. Further,

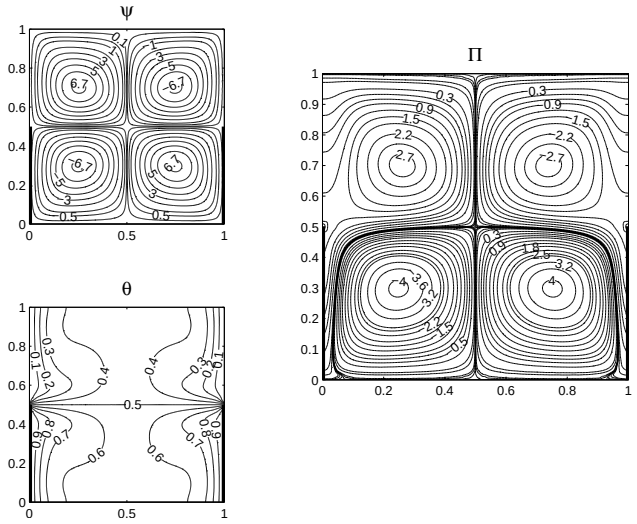

Figure 2: Streamfunctions (ψ), heatfunction (Π) and temperature (θ) plots for $Ra = 10^5$ and $Pr = 7$ for case 1. Clockwise and anti-clockwise flows are shown via negative and positive signs of streamfunctions and heatfunctions, respectively. Thick lines along the vertical walls represent the uniformly heated section while remaining sections are maintained cold.

in addition to end to end heatlines, intense closed loop heatline cells ($|\Pi|_{max} = 4$) are seen due to high convection. It may also be noted that, the intensity of thermal mixing is greater at the bottom halves of the cavity as seen from stronger magnitudes of closed loop heatlines at the lower half. Note that, dense heatlines along the lower half of the enclosure represents internal thermal mixing.

Due to enhanced thermal mixing, isotherms are highly distorted at the top and bottom halves of the cavity. Note that, uniform temperature is maintained with $\theta = 0.4 - 0.6$ throughout the core of the cavity. The presence of dense heatlines along the lower and upper central regions of the enclosure, gives rise to internal thermal mixing near the core region. This causes the temperature to vary within $\theta = 0.5 - 0.6$ in the bottom half whereas the temperature varies within $\theta = 0.4 - 0.5$ in the upper central region. As expected, isotherms are compressed at the hot-cold junction due to temperature singularity. In addition, isotherms are also strongly compressed at the bottom portion and top corners of the side walls signifying very high thermal gradient. This signifies high heat transfer rate in those regions which can also be explained based on dense heatlines.

5.2 Case 2

In this case, uniform heat sources are applied at $0.15 \leq Y \leq 0.65$ for both the vertical walls and the distribution of streamlines, heatlines and isotherms are presented in Fig. 3. As the heat sources are not present within $0 \leq Y \leq 0.2$ along the side walls, a stagnant cold zone is found near the bottom portion of the cavity. The formation of stagnant zone near the bottom portion of the enclosure, is depicted from the smaller magnitude of streamfunction ($|\psi| = 0.1$) near those regions. The primary streamline

cells are observed just above the stagnant fluid zone. Note that, large primary streamline cells with high magnitude ($|\psi|_{max} = 5.5$) are seen near the heaters, as the buoyancy forces are high near those zones. Hot fluid near $Y = 0.65$, rises upwards and flows down along the cold regime of the side walls ($1 \leq Y \leq 0.65$), thus forming secondary circulation cells. Since less area is available for the fluid motion in the upper half of the enclosure, the size and intensity of the secondary circulation cells are smaller for case 2 ($|\psi| = 4.5$) as compared to case 1 ($|\psi| = 6.7$). In addition, the eye of the secondary vortex shifts from the middle region to the upper region due to the vertical shifting of the heaters for the present case in contrast to case 1.

Enhanced convection causes hot regimes of side walls to transfer heat to a larger extent of cold regimes within $0.65 \leq Y \leq 1$ and $0 \leq Y \leq 0.15$. Heatline cells are observed at the upper portion of the cavity as well as near the central region above the bottom wall. The strong convective heatline cells recirculate significant amount of heat as seen by $|\Pi|$ varying within $1.2 - 2$ at the top central portion and $0.6 - 3$ near the center of the enclosure. In contrast to case 1, small tertiary cells ($|\Pi|_{max} = 0.08$) are observed near the bottom wall for case 2. It may be noted that, due to low intensity of streamline cells, the intensity of heatline cells is also less for case 2 ($|\Pi|_{max} = 3.4$) as compared to case 1 ($|\Pi|_{max} = 4$).

As seen from Fig. 3, high temperature gradient is observed in the top portion of side walls ($\theta = 0.1 - 0.5$) as isotherms are compressed towards the side walls. Thus, the thermal boundary layer thickness is reduced significantly within $0.65 \leq Y \leq 1$. Dense heatlines, near the central core at the top and bottom half of the enclosure, represent enhanced thermal mixing in those regions. This results in uniform distribution of temperature within $\theta = 0.5 - 0.6$ near the top central portion of the cavity. Lower portion within $0 \leq Y \leq 0.15$, also receives heat from the hot portion. Overall, the heaters distribute heat uniformly throughout the cavity. Thus, a large central portion of the bottom half is also maintained at $\theta = 0.5 - 0.6$, which contrasts case 1. In addition, isotherms near the hot regimes are highly compressed due to the presence of dense heatlines along the side walls. It is also observed that, the hot regimes transfer heat to the cold regimes near the bottom portion of the side walls. Therefore, θ varies within $0.1 - 0.5$ near the bottom corners of the enclosure. In addition, due to the presence of heaters within $0.15 \leq Y \leq 0.65$ on the side walls, a large central core region of the enclosure is maintained at $\theta = 0.6 - 0.7$.

5.3 Case 3

In this case, heat sources are applied at $0.25 \leq Y \leq 0.75$ along the left and right vertical walls (Fig. 4). As heat sources are now placed at the central portion of side walls, fluid flow in the cavity is altered as depicted by streamlines. It is observed that, stagnation zone near the bottom half of the enclosure covers more area with comparatively higher magnitude ($|\psi| = 1.1$) in contrast to case 2, since the heaters are located within $0.25 \leq Y \leq 0.75$. The intensity of the primary circulation cell situated around the central region of the enclosure, also decreases significantly ($|\psi|_{max} = 4$) as compared to case 2 ($|\psi|_{max} = 5.5$). Although the flow intensity is less at the top portion, the flow strength in other regions are sufficiently stronger to provide mixing effect, which is further illustrated by heatlines.

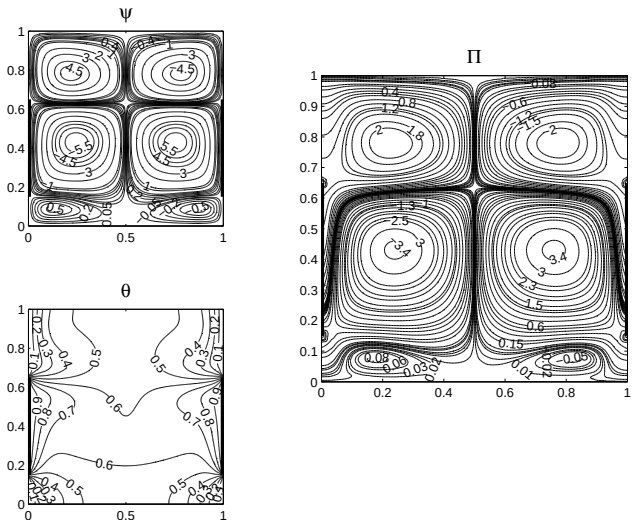

Figure 3: Streamfunctions (ψ), heatfunction (Π) and temperature (θ) plots for $Ra = 10^5$ and $Pr = 7$ for case 2. Clockwise and anti-clockwise flows are shown via negative and positive signs of streamfunctions and heatfunctions, respectively. Thick lines along the vertical walls represent the uniformly heated section while remaining sections are maintained cold.

As heat sources are now placed at the central portion of side walls, circular heatlines, identical to streamlines, are observed apart from end-to-end heatlines at the top and bottom regions. The strong circular heatlines indicate the recirculation of heat energy or the thermal mixing inside the cavity. Heatlines illustrate that the heat distribution in the upper half of the cavity is primarily due to the central heat sources on the side walls as seen via the presence of dense heatlines, depicting large heat transport to the cold top portion of side walls. The heat source at the central region of the enclosure recirculates the heat in the central core region and also transfers heat to the cold regions of the bottom portion of the side walls. Note that, stagnant zone near the bottom corners are responsible for low thermal mixing. However, high thermal gradients are observed near the lower bottom portion, as compared to case 2. It may also be noted that for case 3, the magnitude of primary heatline cell is considerably lower ($|\Pi|_{max} = 2.8$), in contrast to that in case 2 ($|\Pi|_{max} = 3.4$) for identical Ra and Pr (Fig. 4).

Isotherm show high thermal gradient near the top portion of the enclosure as isotherms are compressed due to secondary heatline cells. This signifies enhanced heat flow in those regions. High thermal mixing with $|\Pi| = 1.5$ is observed due to strong convection and therefore the temperature distribution is uniform with $\theta = 0.6 - 0.7$ across a large region near the central and upper portion of the cavity. Dense heatlines near the heat source illustrates large heat transfer rate that gives rise to compressed isotherms near those regions. The thick boundary layer near the bottom portion of the side walls signifies negligible heat flow in that region (Fig. 4). Due to poor heatline circulation or

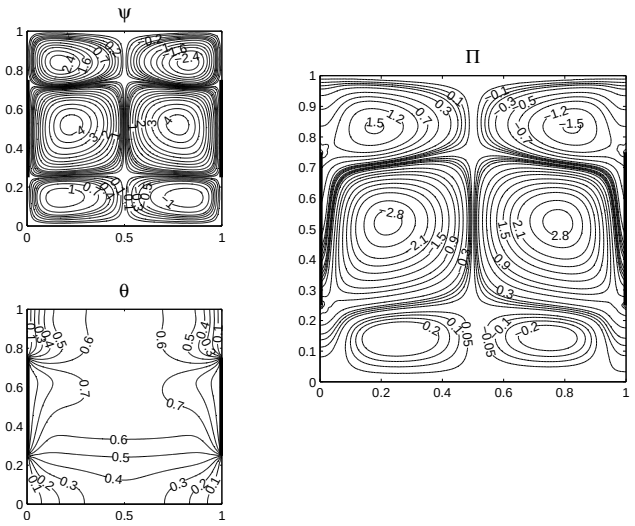

Figure 4: Streamfunctions (ψ), heatfunction (Π) and temperature (θ) plots for $Ra = 10^5$ and $Pr = 7$ for case 3. Clockwise and anti-clockwise flows are shown via negative and positive signs of streamfunctions and heatfunctions, respectively. Thick lines along the vertical walls represent the uniformly heated section while remaining sections are maintained cold

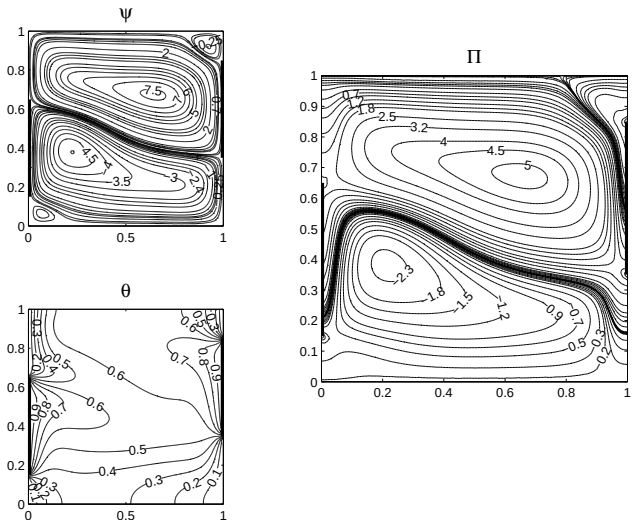

Figure 5: Streamfunctions (ψ), heatfunction (Π) and temperature (θ) plots for $Ra = 10^5$ and $Pr = 7$ for case 4. Clockwise and anti-clockwise flows are shown via negative and positive signs of streamfunctions and heatfunctions, respectively. Thick lines along the vertical walls represent the uniformly heated section while remaining sections are maintained cold.

convective heating at a large zone near the bottom wall, high thermal gradient ($\theta = 0.3 - 0.6$) is observed in those region, indicating poor local thermal mixing.

5.4 Case 4

Fig.6 illustrates streamlines, heatlines and isotherms distributions for $Pr = 7$ and $Ra = 10^5$. In this case, isothermal heat sources are applied at $0.15 \leq Y \leq 0.65$ on the left wall and at $0.35 \leq Y \leq 0.85$ on the right wall. This is an asymmetric configuration in contrast to the previous cases. At $Ra = 10^5$, two large circulation cells of different magnitudes are formed in the upper and lower halves of the enclosure, caused by asymmetric distributed heating. Due to enhanced buoyancy effect, hot fluid from $0.35 \leq Y \leq 0.85$, moves upward in anti-clockwise direction and flows down along $0.65 \leq Y \leq 1$. On the other hand, hot fluid near $0.15 \leq Y \leq 0.65$, rises up due to buoyancy forces but that is intercepted by the movement of the stronger upper circulation cells. This results in the downward clockwise movement of the bottom circulation cell. Note that, due to asymmetric positioning of the heaters, the streamline cells are not circular. It is interesting to observe that, the magnitude of streamfunction ($|\psi|_{max} = 7.5$) in the upper half is more than that of lower half ($|\psi|_{max} = 4.6$). Tiny circulation cells of small magnitude ($|\psi| = 0.25$) are observed near the top right and bottom left corners of the cavity due to negligible fluid flow in the corner regions (see Fig. 6).

As seen from Fig. 5, the streamlines and heatlines in the upper and lower halves of the cavity are observed to be qualitatively similar, which denotes that the heat transport is mainly due to the convective flow in those regions. The heat source of left wall transfers large amount of heat directly to the cold bottom portions of right wall within $0 \leq Y \leq 0.35$. As the bulk of the heat flows towards the cold bottom portion of the right wall, less heat is transferred from the hot regime of left wall to the cold portion above it ($0.65 \leq Y \leq 1$) as seen from the low magnitude of heatfunction ($0.6 \leq |\Pi| \leq 0.8$). However, the upper cold regime on the left wall ($0.65 \leq Y \leq 1$) receives heat corresponding to $0.1 \leq \Pi \leq 1.2$ from the heat sources on the right wall. It may be noted that, the cold regime on the top portion of the right wall ($0.85 \leq Y \leq 1$) receives heat from adjacent hot regime ($0.35 \leq Y \leq 0.85$). It is also found that, the hot regime on the left wall ($0.15 \leq Y \leq 0.65$) transfers smaller amount of heat to the adjacent bottom cold portion ($0 \leq Y \leq 0.15$) as seen from the low magnitude of heatfunctions ($0.2 \leq \Pi \leq 0.4$).

As significant amount of heat is distributed to the upper portion of the left wall ($0.65 \leq Y \leq 1$) from both the heaters, large temperature gradients are observed in those regions leading to the formation of thermal boundary layer and thus the isotherms are found to be compressed at those regions. On the other hand, the cold regime within $0 \leq Y \leq 0.4$ receives heat of low magnitude ($|\Pi| \leq 0.1$) from the heater situated on the left wall ($0.15 \leq Y \leq 0.65$). This leads to the formation of thermal boundary layer of larger thickness along the bottom portion of the right side wall. Due to enhanced thermal mixing and effective heat distribution, the central portion of the upper half of the cavity is uniformly maintained within $\theta = 0.6 - 0.7$ in contrast to the previous cases, at higher Ra. In addition, the presence of dense heatlines near the hot regimes on the vertical walls, result in compressed isotherms ($\theta = 0.6 - 0.9$). Note that, dense heatlines around the central core signify high thermal mixing and uniform temperature distribution with $\theta = 0.5 - 0.6$ (see Fig. 5). In contrast to case 1 and 2, large thermal gradient is observed in the central portion of the bottom half due to poor heatline circulations in the bottom half.

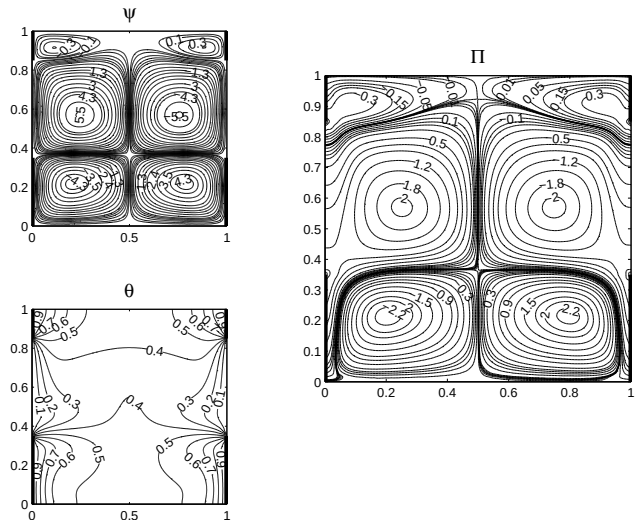

Figure 6: Streamfunctions (ψ), heatfunction (Π) and temperature (θ) plots for $Ra = 10^5$ and $Pr = 7$ for case 5. Clockwise and anti-clockwise flows are shown via negative and positive signs of streamfunctions and heatfunctions, respectively. Thick lines along the vertical walls represent the uniformly heated section while remaining sections are maintained cold.

It may be concluded from the above analysis that, the distributed heating significantly enhances the heat distribution in the cavity. In order to further improve the heat distribution or thermal management in the cavity with the aim of achieving uniform temperature distribution across the cavity, it is proposed to further divide the heat sources and place at various locations along the vertical walls. Detailed investigation of fluid flow and heat distribution in the cavity, with multiple heat sources are presented in the following section.

5.5 Case 5

Fig.7 illustrates the streamlines, heatlines and isotherms distribution for $Pr = 7$ and $Ra = 10^5$ for multiple heat sources on the vertical walls. Isothermal heat sources are applied at $0 \leq Y \leq 0.35$ and $0.85 \leq Y \leq 1$ along each vertical wall (Fig.7). The presence of heaters near $0 \leq Y \leq 0.35$, results in the upward motion of the fluid. However, the fluid does not reach the top portions of the enclosure and tends to flow down and form small circulation cells in the bottom half of the enclosure ($|\psi| = 4.3$). Further, as a result of buoyancy effect, the fluid rises from the zone just above $Y = 0.35$ and flows down along cold portions of the vertical walls ($0.35 \leq Y \leq 0.85$), forming two symmetric rolls in the middle the cavity. Small symmetric circulation cells are also observed near the top corner portions of the enclosure, due to the presence of heaters within $0.85 \leq Y \leq 1$. The intensity of streamlines at the upper portion ($|\psi|_{max} = 5.5$) are stronger compared to those present near the bottom portion of the cavity ($|\psi|_{max} = 4.3$).

The complex patterns of heat flow during the convection mode are adequately illustrated by heatlines. As the heat sources are present along $0 \leq Y \leq 0.35$ on the side walls, strong heatline circulation cells ($|\Pi|_{max} = 2.2$), similar to streamlines, are observed just above the bottom wall. The heat source located at the bottom zone of the side walls ($0 \leq Y \leq 0.35$) also transfers heat to the cold regimes ($0.35 \leq Y \leq 0.8$) of the side walls. Similarly, the heat sources at the upper regions on the side walls ($0.85 \leq Y \leq 1$) transfer heat to a small portion of the cold regimes within $0.8 \leq Y \leq 0.85$. Heatlines are dense near upper portion of the cold side walls ($0.7 \leq Y \leq 0.8$) than at the middle section signifying larger heat flow near $0.7 \leq Y \leq 0.8$. It is interesting to observe that, although the $|\psi|_{max}$ values for the circulation cells at the central and the bottom portions of the cavity are different, the thermal mixing induced by those circulation cells is nearly same as seen from the $|\Pi|_{max}$ values, which are 2.2 and 2 at both the central and bottom portions of the enclosure, respectively (see Fig.7).

Large portion near the central zone in the upper and lower halves are maintained at $\theta = 0.4 - 0.5$, due to enhanced mixing in those regions as visualized from the presence of dense heatlines along the central vertical line of the cavity. Further, the bottom zone also consists of dense heatlines emanating from the heat source signifying large amount of heat flow due to enhanced convection. Thus, the isotherms are largely compressed near the bottom portion of side walls and high temperature gradient is observed. In addition, enhanced thermal mixing near the central core causes the temperature to be maintained within $\theta = 0.3 - 0.4$. The presence of sparse heatlines along $0.35 \leq Y \leq 0.7$ results in the development of boundary layer near those regions. Due to enhanced convection and distributed heating with multiple heat sources, a large portion of cavity is maintained at $\theta = 0.3 - 0.5$, in contrast to case 1. Further, heatlines are more dense near the central region of the cavity within $0.3 \leq Y \leq 0.4$, as compared to case 1. This results in intense heat flow or thermal mixing in those regions, in contrast to that in case 1.

5.6 Case 6

Isothermal hot sources are located at $0 \leq Y \leq 0.15$ and $0.3 \leq Y \leq 0.65$ on each of the side walls (Figure 7). Strong fluid circulation cells ($|\psi|_{max} = 4.3$), representative of enhanced convection, are induced in the cavity due to the presence of multiple heat sources (Fig. 7). Due to intense circulation near the heat source within $0 \leq Y \leq 0.15$, the outer vortex of the primary circulation cell is slightly compressed inward. As a result, the primary fluid circulation cell in this case is not exactly circular. In addition, hot fluid near $Y = 0.65$ rises upwards and flows down along the cold portion of side walls forming symmetric secondary circulation cells ($|\psi| = 3.5$) in the top portion of the cavity. Note that, for the present case, circulation cells near the top corners disappear. Instead, small tertiary cells of low magnitude ($|\psi| = 0.1$) arise near $0.15 \leq Y \leq 0.35$ due to local fluid motion near those regions.

Due to enhanced convection, heatlines are distorted and multiple cells of heatlines are observed. Strong convective cells distribute heat to the top and bottom portions of the cavity. Similar to fluid circulation cells, two primary and two secondary cells of heatlines are also observed. Note that, heatline patterns are qualitatively similar to streamlines. It is interesting to observe that $0.7 \leq Y \leq 1$

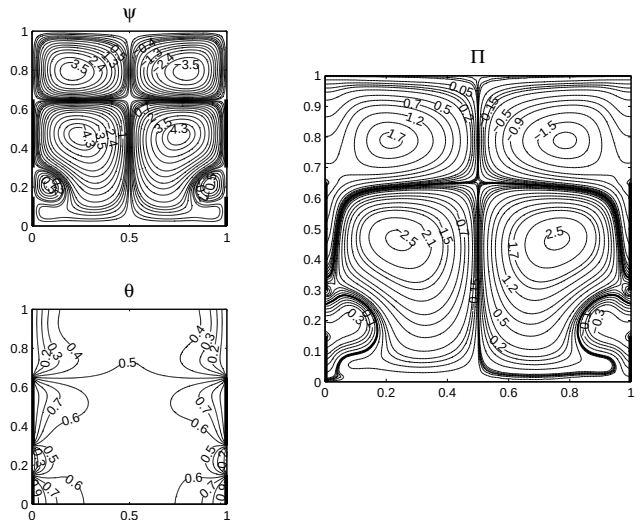

Figure 7: Streamfunctions (ψ), heatfunction (Π) and temperature (θ) plots for $Ra = 10^5$ and $Pr = 7$ for case 6. Clockwise and anti-clockwise flows are shown via negative and positive signs of streamfunctions and heatfunctions, respectively. Thick lines along the vertical walls represent the uniformly heated section while remaining sections are maintained cold.

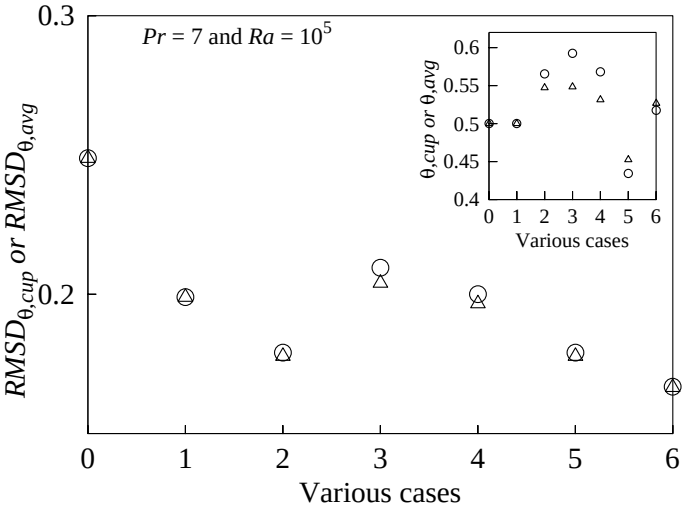

Figure 8: Cup-mixing temperature (◯) and average temperature (△) and root-mean square deviation (RMSD) based on θ_{cup} (◯) and θ_{avg} (△) in various cases for $Pr = 7$ at $Ra = 10^5$.

corresponds to $0.3 \leq \Pi \leq 1$ along the side walls.

Note that, eye of the secondary vortex shifts from the middle region of the cavity to the upper portion of the cavity in contrast to case 5. It is also seen that the dense heatlines occur near $0.3 \leq Y \leq 0.4$, illustrating large heat transport from the heat sources of middle portions of the side wall. In addition, enhanced circulations near the central core region of the enclosure, also denote larger amount of convective heat flow as seen from higher values ($|\Pi|_{max} = 2.5$) of heatfunction (see Fig. 7).

Due to the enhanced thermal mixing, the isotherms near the top portion of the cavity are pushed towards the side walls. Note that, absence of heat source within $0.65 \leq Y \leq 1$ does not necessarily affect the temperature distribution in the top half of the enclosure. As a result, uniform temperature within $\theta = 0.4 - 0.5$ is maintained at the top central region of the cavity, similar to the previous case. Dense heatlines emanating from the hot regimes results in large temperature gradient near $0.3 \leq Y \leq 0.65$ and $0 \leq Y \leq 0.15$ and thus the isotherms are compressed in those regions. In addition, strong convective cells near the centre of the enclosure results in enhanced thermal mixing, due to which, a large portion at the central core is maintained at $\theta = 0.5 - 0.6$ (Fig. 7). Note that, uniform temperature distribution occurs around a large zone near the central and bottom portion of the enclosure which can be explained based on comparatively low thermal gradients in contrast to case 3 and case 4.

5.7 THERMAL MIXING AND TEMPERATURE UNIFORMITY

All the six cases are compared with the conventional differential heating (Case 0) in order to analyze the extent of thermal mixing in the cavity, which indirectly refers to the maximum heat transfer from discrete heat sources to the fluid (Fig. 8). Note that, case 0 refers to the differential heating of the left wall with cold right wall, in the presence of adiabatic top and bottom walls. The cup-mixing temperature (Θ_{cup}) and the spatial average temperature (Θ_{avg}) at $Ra = 10^5$ for each case are evaluated based on Eqs. 21 and 23, respectively and they are illustrated in the inset plots of Fig. 8. Temperature uniformity for various cases is estimated by $RMSD$ based on Θ_{cup} and Θ_{avg} (Eq. 24).

It may be noted that, Θ_{cup} values are shown in the inset plots for various cases at high Ra ($Ra = 10^5$) since it is more suitable when a convective flow exists. It is observed that, $RMSD_{\Theta_{cup}}$ value for case 0 is the highest (= 0.2489) among all the cases. This is evident from the fact that, in differential heating, fluid near the left wall, receives maximum heat which results in the formation of hot spots near the left half of the enclosure. On the other hand, fluid near the right wall remains cold and thus, cold spots tend to occur near the right wall which causes non-uniform temperature distribution throughout the cavity. However, thermal mixing is found to be significant as implied from the value of Θ_{cup} ($\Theta_{cup} = 0.5$) for case 0. Further, it is interesting to observe that, for case 1 and 6, the cup-mixing temperature (Θ_{cup}) closely follows the average temperature (Θ_{avg}). Cup-mixing temperature (Θ_{cup}) in case 2 is found to be 0.5655, which is mainly due to enhanced thermal mixing induced by the distributed heating sources. This can also be verified through the presence of dense heatlines near the central portion of the enclosure ($0.5 \leq |\Pi| \leq 1.3$). Further, low values of $RMSD_{\Theta_{cup}}$ signify high temperature uniformity throughout the enclosure in case 2. However, non-uniformity is observed to be large in case 3 as $RMSD_{\Theta_{cup}}$ is higher (= 0.2095) as compared to case 1 and 2. This may be attributed to the fact that, the lower corners and the region around the bottom middle portion along the center axis, receives negligible amount of heat, as viewed from presence of sparse heatlines ($|\Pi| = 0.05 - 0.1$) for case 3. As a result, the bulk of fluid in that portion

remains cold. Note that, corresponding Θ_{cup} for case 3 is found to be 0.592, which is highest among all the cases (see figure 8). This may be due to the central positioning of the heater source on the vertical walls, which greatly enhances the thermal mixing inside the cavity, as seen from the high intensities of heatlines in those region ($|\Pi|_{max} = 2.8$). On the other hand, presence of dense heatlines near the central, bottom and upper portion of the enclosure, for case 4 (asymmetric configuration), results in high thermal mixing ($\Theta_{cup} = 0.568$) throughout the cavity. However, temperature distribution inside the cavity ($RMSD_{\Theta_{cup}} = 0.2$) does not show much improvement since the bottom corners of the enclosure in case 4 receive negligible amount of heat. For case 6, dense heatlines in the bottom and central zones of the enclosure ($|\Pi|_{max} = 2.52$), indicates adequate distribution of heat throughout the cavity and thus high thermal mixing ($\Theta_{cup} = 0.5174$) is observed. Further, the $RMSD_{\Theta_{cup}}$ value for case 6 is found to be the lowest (= 0.167) among all cases which implies high degree of temperature uniformity inside the enclosure. Thus, it may be concluded that, the distributed heating with case 6 may be an attractive option for processing of fluids, as this configuration results in optimum thermal mixing as well as greater uniformity in temperature distribution across a large region in the cavity.

6 CONCLUSION

The main objective of the present work is to study natural convection in square cavities filled with fluid having $Pr = 7$ due to differential and distributed heating methodologies and analyze their role in enhancing the thermal mixing and temperature uniformity. Overall six cases were considered in the present study and detailed analysis of fluid flow and heat flow have been carried out via streamlines, isotherms and heatlines. Heatline approach has been extensively used to visualize thermal mixing and the complex heat flow patterns in the cavity.

In all the cases, at $Ra = 10^3$, it is found that heatlines are smooth curves, perpendicular to isothermal surfaces, parallel to adiabatic surface and are of low magnitudes. These characteristics of heatline represent conduction dominant heat transfer. At $Ra = 10^5$, heatlines are distorted and magnitudes are increased, signifying enhanced heat transfer due to dominant convection mode. In addition, thermal mixing throughout the cavity is evaluated and visualized via heatlines. In case 1, it is observed that, larger regime of the heat source is located near the bottom of the side walls due to which less heat is transferred to the upper portion of the cavity. For case 2, the heat sources are shifted slightly upward along the vertical walls thus giving rise to stagnant cold spots near the bottom corners. However, improved temperature uniformity is observed throughout the cavity with significant thermal mixing. In case 3, the heat sources are centrally located on the vertical walls. Although, heat distribution to the upper zone of the cavity is largely enhanced, temperature non-uniformity prevails throughout the enclosure due to poor convection near the bottom zone. In case 4, it is observed that the heat source on the left vertical wall transfers heat to the bottom portion of the right wall, while heat source on the right vertical wall supply heat to the top cold regime of the left and right vertical wall. This results in non-uniform temperature distribution throughout the cavity. For case 5, multiple heat source provides high temperature uniformity but comparatively with low thermal mixing. Case 6 configuration is the best among all the cases since it gives the highest temperature uniformity with significant thermal mixing.

Overall, the heatline approach establishes that the distributed heating is more efficient than conventional differential heating. Also, the present work illustrates that distributed heating is an energy saving alternative as compared to differential heating.

REFERENCES

[1] Deng Q.H., and Tang G.F., Numerical visualization of mass and heat transport for conjugate natural convection/heat conduction by streamline and heatline, *International Journal of Heat and Mass Transfer*, Vol. 45, 2002, pp. 2373-2385

[2] Ilis G.G., Mobedi M., and Sunden B., Effect of aspect ratio on entropy generation in a rectangular cavity with differentially heated vertical walls, *International Communications in Heat and Mass Transfer*, Vol. 35, 2008, pp. 696-703

[3] Hossain M.A., Asghar S., and Gorla R.S.R., Buoyancy-driven flow of a viscous incompressible fluid in an open-ended rectangular cavity with permeable horizontal surfaces, *International Journal of Numerical Methods and Fluid flow*, Vol. 20, 2010, pp. 759-772

[4] Keyhani M., Prasad V., and Cox R., An experimental study of natural convection in a vertical cavity with discrete heat sources, *ASME Journal of Heat Transfer*, Vol. 110, 1988, pp. 616-624

[5] Polentini M.S., Ramadhyani S., and Incropera F.P., Single phase thermosyphon cooling of an array of discrete heat sources in a rectangular cavity, *Int. J. Heat Mass Transfer*, Vol. 36, 1993, pp. 3983-3996

[6] Plumat E., Development and prospectives of furnaces for glass melting, *Journal of Non-Crystalline Solids*, Vol. 26, 1977, pp. 183-261

[7] Sarris I.E., Lekakis I., and Vlachos N.S., Glass Melt Recirculation Controlled by a Heated Strip in the Tank Bottom, *Proceedings of the First Balkan Conference on Glass*, Volos, Greece, 2000, pp.379-388

[8] Mariani V.C., and Coelho L.S., Natural convection heat transfer in partially open enclosures containing an internal heat source, *Brazilian Journal of Chemical Engineering*, Vol. 24, 2007, pp. 375 - 388

[9] Kimura S., and Bejan A., The heatline visualization of convective heat-transfer, *Journal of Heat Transfer-Trans. ASME*, Vol. 105, 1983, pp. 916-919

[10] Reddy J.N., An introduction to the finite element method, *McGraw-Hill, New York*, 1993

[11] Basak T., Roy S., and Balakrishnan A.R., Effects of thermal boundary conditions on natural convection flows within a square cavity, *International Journal of Heat and Mass Transfer*, Vol. 49, 2006, pp. 4525-4535

[12] Basak T., and Roy S., Role of 'Bejans heatlines' in heat flow visualization and optimal thermal mixing for differentially heated square enclosures, *International Journal of Heat and Mass Transfer*, Vol. 51, 2008, 3486-3503